02

Influence of Flux and Ho^{3+} Doping Concentration on Upconversion Luminescent Performance of $BaGd_2ZnO_5:Er^{3+}/Yb^{3+}$ Phosphors under 980 nm Laser Excitation

© Shengyi Liu[1], Duan Gao[2], Li Wang[1], Yongfeng Zhang[1], Wenbin Song[1], Jun Huang[1], Qianmiao Yu[1], Yongbo Wen[1], Qi Zhang[1], Peijia Xiao[1]

[1] School of Intelligence and Electronic Engineering, Dalian Neusoft University of Information, 116026 Dalian, Liaoning, China
[2] College of Science, Dalian Maritime University, 116026 Dalian, Liaoning, China

e-mail: liushengyi@neusoft.edu.cn

Received September 26, 2023
Revised September 26, 2023
Accepted November 23, 2023

Utilizing the conventional high-temperature solid-phase method, two sets of $BaGd_2ZnO_5$ phosphors were synthesized with fixed Er^{3+}/Yb^{3+} concentrations while varying the flux and Ho^{3+} concentrations. XRD results confirmed that the obtained products were all pure-phase $BaGd_2ZnO_5$, with no alterations in crystal phases observed with varying levels of Ho^{3+} doping and different flux agents. Employing 980 nm as the excitation source, upconversion emission spectra of the samples were recorded under identical conditions. The relationship between the upconversion luminescence intensity of the Ho^{3+}-doped samples and the laser working current was investigated. Analysis using the intensity-constraining formula revealed that both red and green upconversion emissions in the samples were two-photon processes. Additionally, the energy transfer processes involved were explored. The temperature effect on the $Er^{3+}/Yb^{3+}/Ho^{3+}$ tri-doped samples was also examined, and the activation energy of the samples was calculated.

Keywords: High temperature solid phase, upconversion, Flux, 980 nm Laser.

DOI: 10.61011/EOS.2023.11.58046.128-23

1. Introduction

Recently, due to the outstanding luminescent properties of up-conversion, it has received widespread attention from researchers. Up-conversion luminescence is a nonlinear optical process that involves absorbing at least two photons and emitting them as light with a shorter wavelength than the excitation wavelength [1–3]. This is also known as anti-Stokes emission. Up-conversion luminescent materials convert infrared radiation into ultraviolet light or visible light. Up-conversion luminescence finds wide applications in various industries, including solid-state lighting, semiconductor displays, biomedical imaging, multicolor displays, fluorescent probes, and markers [4–8], among other fields. The choice of host material for up-conversion luminescence is crucial. In recent years, various fluoride materials with low phonon energy have been reported, but fluoride materials exhibit unstable chemical and physical properties [9,10]. Recent literature has reported that compounds with the AB_2CO_5 structure possess excellent physical and chemical properties, optical properties, and superconducting properties [11,12]. Particularly, $BaGd_2ZnO_5$, as one of the members, has been demonstrated as an effective up-conversion luminescent host material. Among the various rare earth ions studied for up-conversion luminescence, Ho^{3+} has attracted interest from researchers due to its long-lived intermediate metastable states, electronic states, and well-spaced energy levels arising from $f-f$ transitions [13–16]. Additionally, Yb^{3+} serves as an excellent sensitizer for Ho^{3+} because it exhibits a large absorption cross-section near 980 nm and can compensate for the small absorption cross-section of Ho^{3+} [17–20].

Up-conversion luminescence involves a complex luminescent process, and the properties of the luminescent centers are influenced by various external factors, such as different synthesis temperatures, the selection of different host materials, and different doping concentrations of rare earth ions [21]. Among these factors, according to a review of multiple papers related to up-conversion luminescence, it is found that the doping concentration of rare earth ions has a significant impact on up-conversion luminescence [22–24]. However, for various commonly used rare earth ions like Yb, achieving the maximum up-conversion luminescence intensity becomes challenging with high doping concentrations and co-doping with multiple rare earth ions. Even achieving the best results with a small number of experiments is infeasible. Therefore, finding an efficient and precise experimental method to obtain the optimal doping concentration of co-doped ions has become one of the hotspots and challenges in the research field [25–28].

The experimental optimization design method is an efficient and convenient way to obtain comprehensive experimental points [29,30]. The commonly used methods for experimental optimization design are uniform design

and second-order general rotational combination design. Arranging the experimental plan using uniform design not only allows for the preliminary optimization of the samples but also enables accurate conclusions with the fewest number of applied experimental points. The second-order general rotational combination design encodes actual factors into the coding space using a natural factor coding table. Based on the rotational and generality properties of the binary quadratic regression model, it reduces the number of experimental points with the most accurate basis and ensures the accurate prediction of the regression equation for the results.

Although the up-conversion luminescence process of $BaLa_2ZnO_5$: Er^{3+}, Yb^{3+} has been reported, employing an experimental optimization method for material synthesis and research is a more scientific approach. Firstly, a combination of uniform design and second-order general rotational combination design is used to optimize the up-conversion luminescent material co-doped with rare earth ions throughout the entire process. The experimental factors chosen are Er^{3+}/Yb^{3+}, and the fluorescent powder is prepared using the high-temperature solid-phase method. The uniform design method is used for the preliminary optimization of the luminescence intensity. Subsequently, further experimental design is conducted through the second-order general rotational combination design. A binary quadratic regression equation is established, and a genetic algorithm is applied for solution to obtain the maximum luminescence intensity of the sample, along with the optimal concentration. The optimal sample is prepared using the high-temperature solid-phase method, and the crystal structure, up-conversion luminescence spectrum, temperature effect on up-conversion luminescence, and the mechanism of up-conversion luminescence are studied.

In order to obtain the strongest luminescence of rare earth-doped zinc salts for up-conversion, an experimental optimization design method was applied to comprehensively optimize the entire experiment. The theoretical value of the maximum red light emission intensity obtained was $y_{\text{red}} = 70699.53$, with Er^{3+}/Yb^{3+} doping concentrations of $z_1 = 3.121$ mol%, $z_2 = 14.999$ mol% [31]. Based on this, the addition of flux and Ho^{3+} ions were introduced to enhance its luminescence intensity.

In this study, a series of $BaGd_2ZnO_5$ phosphors with different doping concentrations of H_3BO_3, LiF, and Ho^{3+} ions were synthesized using the high-temperature solid-phase reaction method. XRD analysis was used for phase analysis of the samples. The up-conversion emission spectra of samples with different doping concentrations were tested under excitation of a 980 nm laser. The influence of flux and Ho^{3+} doping concentration on up-conversion luminescence intensity was studied. The temperature effect on the samples was explored, showing a decrease in emission intensity with increasing temperature, indicating the occurrence of temperature quenching. The activation energy of the samples was calculated, and the up-conversion luminescence mechanism under different concentrations of Ho^{3+} was discussed.

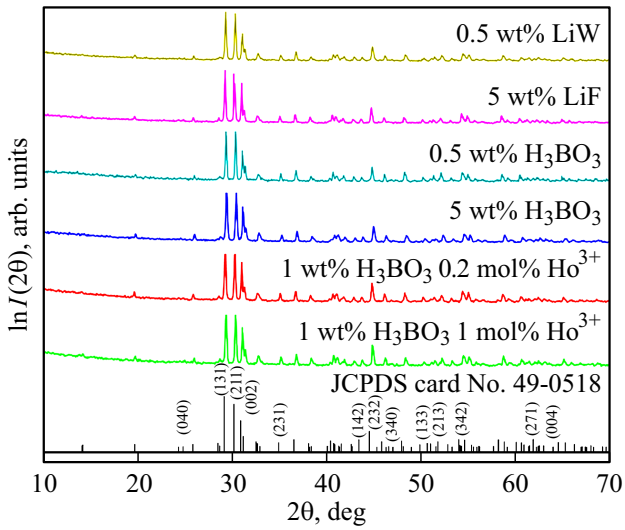

Figure 1. XRD patterns of $BaGd_2ZnO_5$ samples and comparison with JCPDS card No. 49-0518 data.

2. Experimental section

The preparation of samples used analytical pure LiF, $BaCO_3$, ZnO, H_3BO_3, Gd_2O_3, Ho_2O_3, Yb_2O_3, Er_2O_3 as raw materials. The stoichiometric ratios of each reactant were calculated for each doping concentration, and the required masses of each reactant were accurately weighed using an electronic balance. The $BaGd_2ZnO_5:Er^{3+}/Yb^{3+}$ samples were synthesized using the high-temperature solid-phase method. Different concentrations of flux LiF and H_3BO_3 were added to the sample with the maximum red light emission intensity ($BaGd_2ZnO_5$: 3.121 mol% Er^{3+}/14.999 mol% Yb^{3+}), with design concentrations of 0, 0.5 wt%, 1 wt%, 2 wt%, and 5 wt%. Another set of doped samples had fixed Er^{3+} doping concentration of 3.121 mol% and Yb^{3+} doping concentration of 14.999 mol%, while Ho^{3+} doping concentrations were 0, 0.2 mol%, 0.5 mol%, and 1 mol%.

The crystal structures of the fabricated samples were characterized employing a powder X-ray diffractometer (XRD-6000, Shimadzu Japan) equipped with Cu Kα radiation ($\lambda = 1.54$ Å). Photoluminescence spectroscopy (PL) and photoluminescence excitation spectroscopy (PLE) were conducted using a fluorescence spectrometer (F4600, Hitachi, Japan). The afterglow attenuation curve, fluorescence lifetime, and quantum yield of the phosphors were evaluated employing a transient steady-state fluorescence spectrometer (FLS1000, Edinburgh, UK).

3. Results and discussion

3.1. Crystal structure characterization of samples

To identify the crystal structure of the obtained samples, XRD patterns were tested, and it was observed that the diffraction patterns of the samples were nearly

identical. Figure 1 presents the XRD diffraction patterns of BaGd2ZnO5: 3.121 mol% Er^{3+}/14.999 mol% Yb^{3+} samples doped with 0.5 wt% LiF, 5 wt% LiF, 0.5 wt% H_3BO_3, and 5 wt% H3BO3. The XRD diffraction patterns of the three-doped $BaGd_2ZnO_5$: 3.121 mol% Er^{3+}/14.999 mol% Yb^{3+} and samples doped with 0.2 mol% Ho^{3+} and 1 mol% Ho^{3+} are also shown. By comparing the diffraction peaks in the standard card (JCPDS No.49-0518) with the diffraction peaks of the samples, it can be observed that the diffraction peaks from the standard card and the sample nearly coincide. No other impurity diffraction peaks were observed in the diffraction patterns of the samples, indicating that pure-phase $BaGd_2ZnO_5$ samples were obtained. Additionally, this result suggests that the addition of flux aids in the crystallization of the samples, and the variation in doping concentration of the trivalent rare earth ions did not alter the crystal structure of the samples, likely due to the similar valence states and close ionic radii of Gd^{3+}, Er^{3+}, Yb^{3+}, and Ho^{3+} ions [32,33].

3.2. Influence of LiF doping concentration on up-conversion luminescence of $BaGd_2ZnO_5$: 3.121 mol% Er^{3+}/14.999 mol% Yb^{3+} phosphors

The effect of changing LiF doping concentration on up-conversion luminescence of $BaGd_2ZnO_5$: 3.121 mol% Er^{3+}/14.999 mol% Yb^{3+} samples was investigated. The up-conversion emission spectra of samples with different doping concentrations were tested under excitation of a 980 nm laser. Figure 2 shows the spectra obtained from samples with varying LiF doping concentrations. In the figure, a strong red emission center is observed at 662 nm, corresponding to the transition $^4F_{9/2} \rightarrow {}^4I_{15/2}$. Two strong green emission centers appear at 551 nm and 527 nm, corresponding to the transitions $^4S_{3/2} \rightarrow {}^4I_{15/2}$ and $^2H_{11/2} \rightarrow {}^4I_{15/2}$, respectively. Additionally, a weak blue emission at 410 nm is observed, corresponding to the transition $^4F_{7/2} \rightarrow {}^4I_{15/2}$. The inset in Fig. 2 shows the relationship between the integrated up-conversion intensity of red and green light with varying LiF concentration. It can be observed that both the red and green light intensities increase with the LiF concentration. When the LiF doping concentration is 1 mol%, the red and green light of the sample reach their maximum emission intensity. With further increases in LiF doping concentration, the emission intensity of both red and green light decreases, a phenomenon similar to concentration quenching occured in the up-conversion material.

3.3. Influence of H3BO3 doping concentration on up-conversion luminescence of $BaGd_2ZnO_5$: 3.121 mol% Er^{3+}/14.999 mol% Yb^{3+} phosphors

Samples with varying H3BO3 doping concentrations were tested for up-conversion emission spectra under equivalent conditions. The results obtained are shown in Fig. 3. Similar to Fig. 2, the $BaGd_2ZnO_5$: 3.121 mol% Er^{3+}/14.999 mol% Yb^{3+} phosphors doped with different concentrations of flux (LiF, H_3BO_3) showed blue, green, and red up-conversion luminescence. The intensities of red and green up-conversion luminescence were significantly enhanced. The inset in Fig. 3 shows the relationship between the integrated up-conversion intensity of red and green light and the H_3BO_3 doping concentration. It can be seen that, with increasing H_3BO_3 concentration, both red and green light up-conversion intensities initially increase and then reach their maximum emission intensity at an H_3BO_3 doping concentration of 1 mol%. The intensities of both red and green light decrease with further increases in H_3BO_3 doping concentration, indicating a phenomenon similar to concentration quenching occured in the up-conversion material. One of the contributing factors to this phenomenon is the aggregation effect. The aggregation effect refers to the potential clustering of rare earth ions with the increase of the cosolvent. This clustering may lead to a shortened distance between ions, thereby increasing the likelihood of non-radiative energy transfer, similar to the effects observed in concentration quenching. Another possible reason could be attributed to electronic interactions, where with the addition of cosolvent, the interactions between electrons may undergo changes. These changes may include electron cloud overlap and electron transfer, impacting the energy transfer between luminescent centers, akin to the effects seen in concentration quenching.

3.4. Effect of Ho^{3+} doping concentration on up-conversion luminescence of ternary-doped BaGd2ZnO5 phosphors

Figure 4 presents the up-conversion emission spectra of BaGd2ZnO5 samples under the excitation of a 980 nm laser. The $BaGd_2ZnO_5$ samples had fixed Er^{3+}/Yb^{3+} doping concentrations of 3.121 mol% Er^{3+}/14.999 mol% Yb^{3+} and varying Ho^{3+} doping concentrations. The inset in Fig. 4 shows the relationship between the integrated up-conversion intensity of red and green light and the Ho^{3+} doping concentration. It is observed that, with an increase in Ho^{3+} doping concentration, the red light up-conversion intensity of the sample decreases. Furthermore, the green light up-conversion intensity initially increases and then decreases, reaching its maximum value at an Ho^{3+} doping concentration of 0.2 mol%. From the results of the up-conversion luminescence in the previous three groups of samples, it can be seen that the blue and near-infrared emissions are very weak, while the green and red emissions are both strong.

3.5. Constraints on up-conversion luminescence intensity of Er^{3+}/Yb^{3+}/Ho^{3+} ternary-doped $BaGd_2ZnO_5$ Phosphors and up-conversion luminescence mechanism

Under equivalent experimental conditions, the up-conversion emission spectra of samples with different Er^{3+}/Yb^{3+}/Ho^{3+} ternary doping concentrations were tested under varying working currents of a 980 nm laser. Figure 5

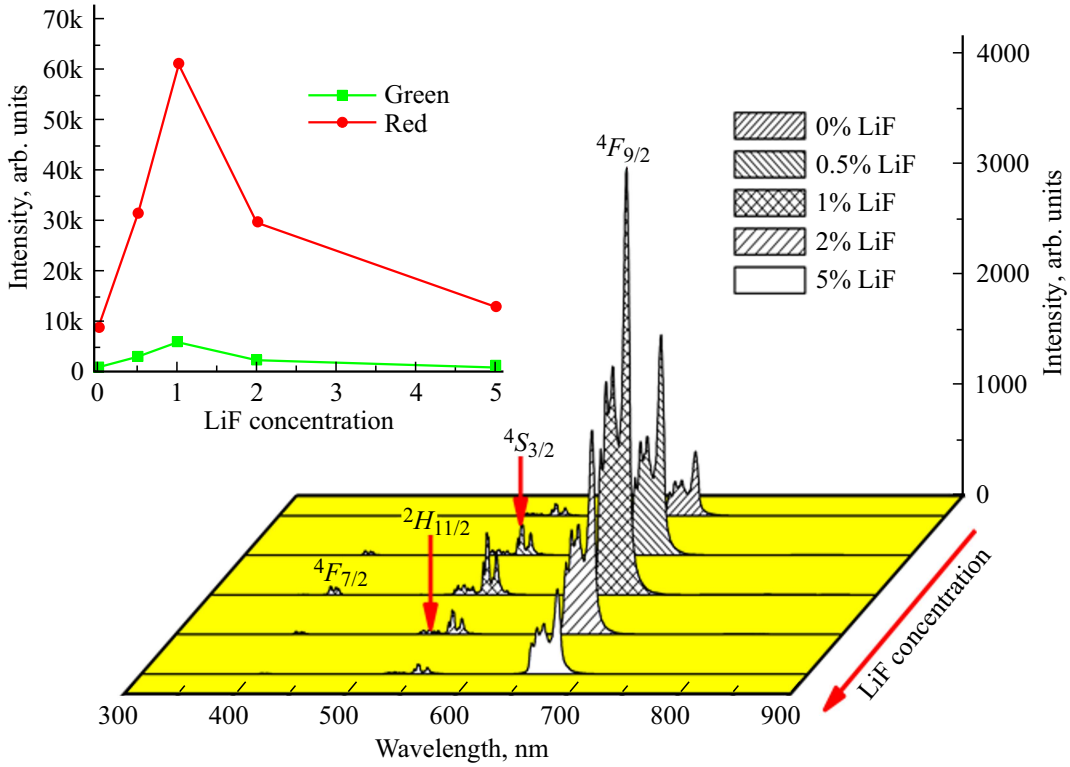

Figure 2. Up-conversion emission spectra of samples with different LiF dopant levels. The inset graph illustrates the relationship between integrated red and green up-conversion intensities and LiF concentration.

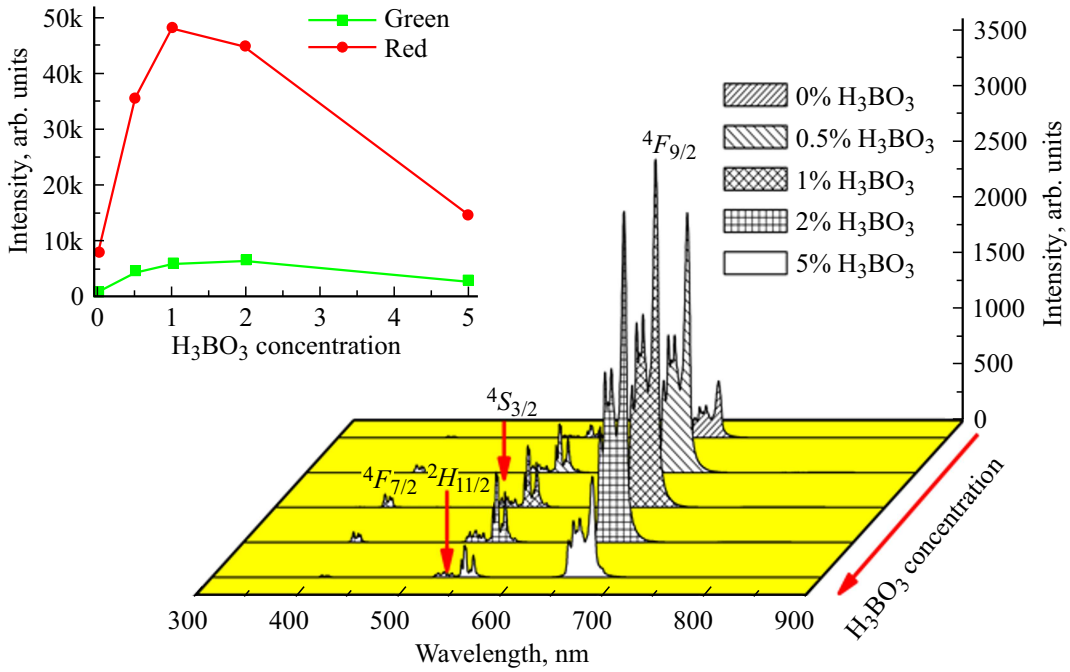

Figure 3. Up-conversion emission spectra of samples with varied H3BO3 dopant levels. The inset graph demonstrates the relationship between integrated red and green emission intensities and H3BO3 concentration.

displays the up-conversion emission spectra of the sample doped with 3.121 mol% Er^{3+}/14.999 mol% Yb^{3+}/1 mol% Ho^{3+} at different laser currents. The inset in Fig. 5, *a* shows the normalized emission intensity for $^4S_{3/2} \rightarrow {}^4I_{15/2}$ and $^5S_2 \rightarrow {}^5I_8$. It can be observed from the emission spectra that the normalized emission intensity for $^2H_{11/2} \rightarrow {}^4I_{15/2}$

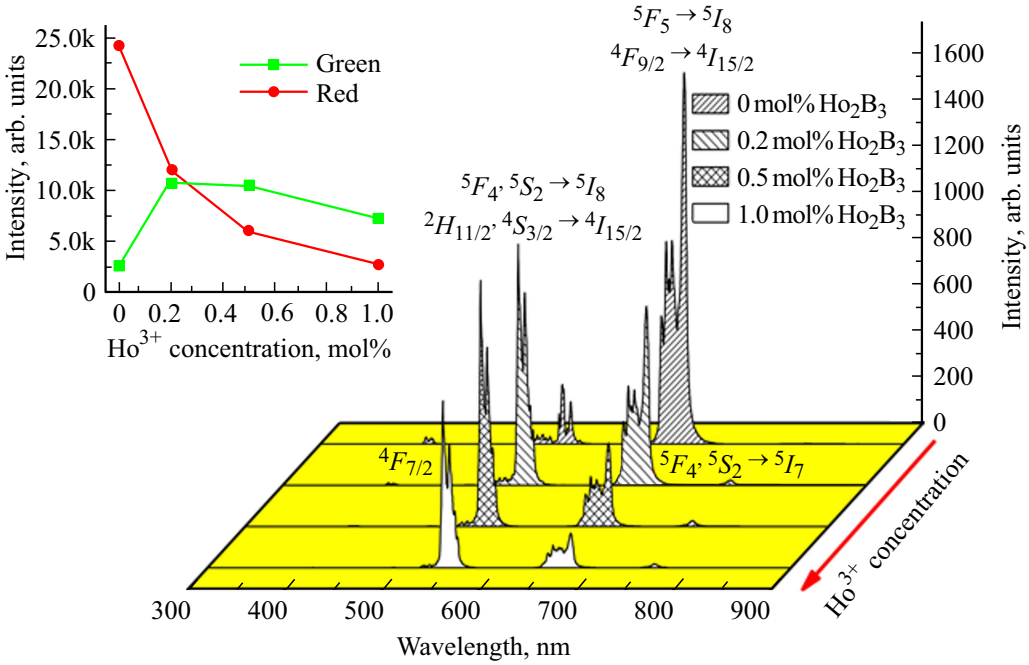

Figure 4. Up-conversion emission spectra of samples with different Ho^{3+} doping levels. The insert graph illustrates the relationship between integrated red and green intensities and Ho^{3+} concentration.

and ${}^5F_4 \rightarrow {}^5I_8$ remains nearly constant, indicating that the effect of laser irradiation on the temperature change of the up-conversion sample can be disregarded under this excitation density [33,34]. The relationships between the laser current and the integrated up-conversion emission intensity are shown in the inset of Fig. 5, *b*. The experimental curves are represented by the dotted lines, and the fitted curves represented by solid lines are obtained using the following equation:

$$I = b(i - i_0)^n. \qquad (1)$$

The fitted values of n are close to 2, indicating that the up-conversion emission of red and green light in the $Er^{3+}/Yb^{3+}/Ho^{3+}$ ternary-doped sample is a two-photon process.

3.6. Discussion on the up-conversion luminescence mechanism of $Er^{3+}/Yb^{3+}/Ho^{3+}$ ternary-doped BaGd2ZnO5 phosphors

The study of the up-conversion luminescence intensity constraints for $Er^{3+}/Yb^{3+}/Ho^{3+}$ ternary-doped $BaGd_2ZnO_5$ phosphors under excitation by a 980 nm laser suggests that the up-conversion process for samples doped with varying concentrations is a two-photon process. Moreover, many studies have already investigated the two-photon up-conversion mechanism for $Er^{3+}/Yb^{3+}/Ho^{3+}$ ternary-doped luminescent materials. As shown in Fig. 6, to achieve red and green up-conversion emission, the process likely involves energy transfer from Er^{3+} to Ho^{3+} through processes such as ground-state absorption (GSA) of Er^{3+} and Ho^{3+}, excited-state absorption (ESA) of Er^{3+} and Ho^{3+}, and energy transfer (ET) from Yb^{3+} to Er^{3+} and Yb^{3+} to Ho^{3+}. In this process, Yb^{3+} ions act as sensitisers, transferring energy to Er^{3+} and Ho^{3+} ions. It can be observed from Fig. 4 that the red emission intensity continuously decreases, while the green emission intensity firstly increases and then decreases. This may be attributed to cross-relaxation processes of Er^{3+} $[({}^4F_{7/2} + {}^4I_{15/2}) \rightarrow ({}^4I_{11/2} + {}^4I_{11/2})]$ and $[({}^4I_{13/2} + {}^4F_{9/2}) \rightarrow ({}^4I_{11/2} + {}^4I_{9/2})]$ and Ho^{3+} $[({}^5S_2, {}^5F_4 + {}^5I_7) \rightarrow ({}^5F_5 + {}^5I_6)]$. Detailed energy transfer processes are illustrated in Fig. 6.

3.7. Influence of temperature on up-conversion luminescence of $Er^{3+}/Yb^{3+}/Ho^{3+}$ ternary-doped $BaGd_2ZnO_5$ phosphors

Figure 7 presents the up-conversion emission spectra of the sample doped with 3.121 mol% Er^{3+}/14.999 mol% Yb^{3+}/1 mol% Ho^{3+} at different temperatures under a 980 nm laser. It is observed that, with increasing temperature, the up-conversion emission intensities of red, green, and near-infrared light gradually decrease, indicating the occurrence of temperature quenching. The inset of Fig. 7 shows the relationship between the luminescent intensities and temperature changes. The black scattered points represent the integrated luminescent intensity of the entire sample with varying temperature. The green points represent the luminescent intensity of the green component, and the red points represent the luminescent intensity of the red component. The experimental data points were fitted

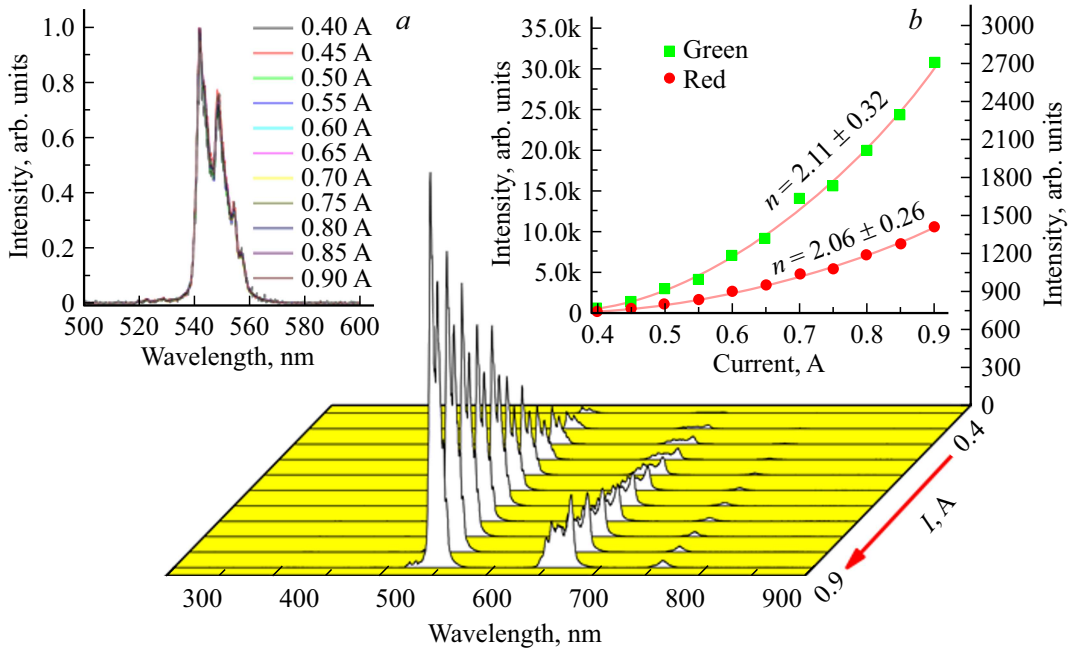

Figure 5. Influence of fiber laser working current on up-conversion emission intensity of optimal samples. Insets (*a*) display the relationship between integrated red and green up-conversion intensities and laser working current, with experimentally measured data represented by dotted lines. Insets (*b*) present normalized up-conversion spectra at different laser working currents.

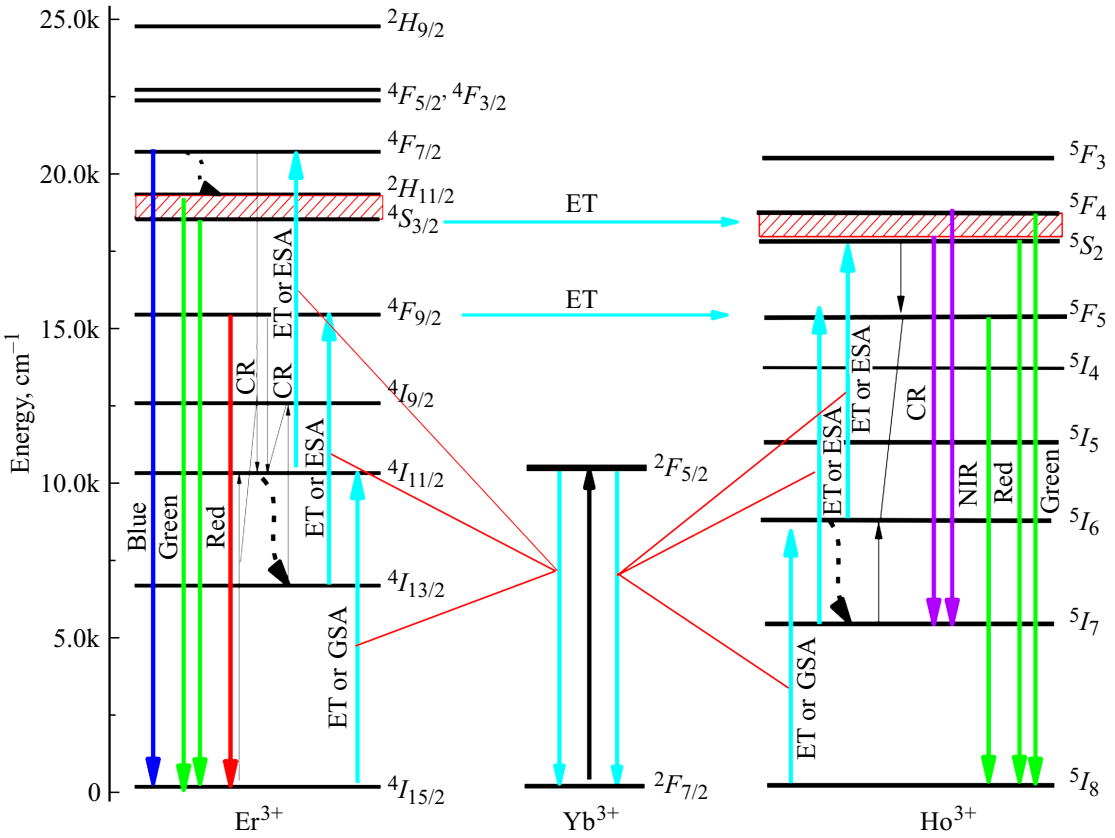

Figure 6. Up-conversion mechanism for elucidating the luminescence process in $BaGd_2ZnO_5$: $Er^{3+}/Yb^{3+}/Ho^{3+}$ samples.

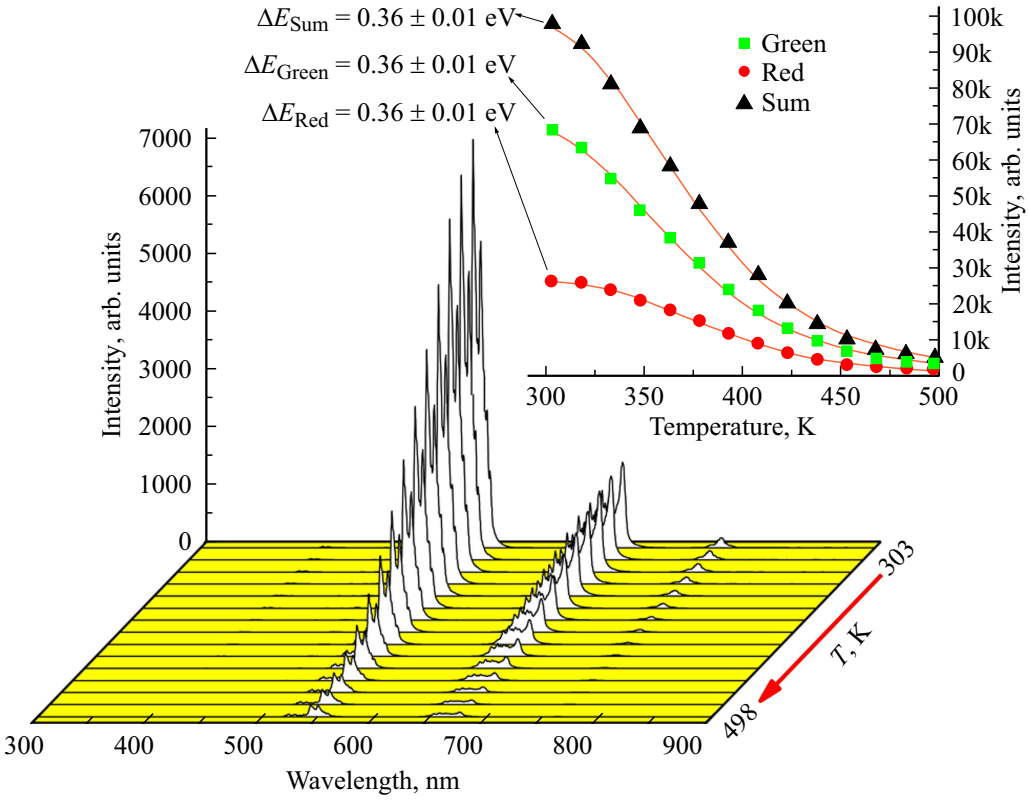

Figure 7. Up-conversion emission spectra of the optimal sample recorded at various temperatures. The inset displays the correlation between luminescence intensity and sample temperature, with the red solid line representing the fitting curve.

using the following equation:

$$I(T) = \frac{I_0}{1 + Cg\exp\left(\frac{-DeltaE}{kT}\right)}. \qquad (2)$$

In the formula, I_0 is the initial intensity, $I(T)$ is the luminescence intensity at a given temperature, C is the frequency factor of the radiation transition, k is the Boltzmann constant, and ΔE is the activation energy of the thermal quenching process [33,34].

Obtaining the fitted curves represented by the red lines. Ultimately, the activation energy for overall luminescence, green light, and red light were determined to be $\Delta E_{Sum} = 0.36$ eV, $\Delta E_{Green} = 0.36$ eV, and $\Delta E_{Red} = 0.36$ eV, respectively.

4. Conclusions

Through traditional high-temperature solid-phase methods, $BaGd_2ZnO_5$ phosphors doped with fixed Er^{3+}/Yb^{3+} concentrations and varying flux additives (LiF, H_3BO_3) were synthesized, as well as ternary-doped $BaGd_2ZnO_5$ phosphors with varying Ho^{3+} concentrations. XRD testing confirmed that all samples with different doping concentrations were of single-phase, and doping concentration did not affect the crystal phase structure of the doped samples. Under 980 nm laser excitation, the up-conversion emission spectra of the doped samples were tested. It was observed that with the addition of flux additives LiF and H3BO3, the red and green up-conversion luminescence intensities of the samples increased. For samples with fixed Er^{3+}/Yb^{3+} concentrations and varying Ho^{3+} concentrations, the red light up-conversion intensity of the ternary-doped sample continuously decreased, while the green light up-conversion intensity firstly increased and then decreased. The blue and near-infrared emissions were weak, whereas the green and red emissions were strong in all three groups of samples.

Acknowledgement

This work is supported by Funds supported by the National Natural Science Foundation of China (approval number: 52201065).

References

[1] Q. Shao, H. Lin, Y. Dong, Y. Fu, C. Liang, and J. He, J. Solid State Chem., 72–77, 225 (2015).
[2] X. Liu, J. Zhang, X. Zhang, Z. Hao, J. Qiao, and X. Dong, Opt. Lett., 148–150, 38 (2013).
[3] F. Liu, W. Yan, Y.J. Chuang, Z. Zhen, J. Xie, and Z. Pan, Sci. Rep., 1554–1563, 3 (2013).
[4] X. Yu, T. Wang, X. Xu, D. Zhou, and J. Qiu, ECS Solid State Lett., R4–R6, 3 (2013).

[5] X. Xu, Q. He, and L. Yan, J. Alloys Compd., 22–26, 574 (2013).
[6] A. McAulay, J. Wang, and C. Ma, Proc. SPIE, 271–276, 77 (1989).
[7] Z. Wen, N.H. Farhat, and Z.J. Zhao, Appl. Opt., 7251–7265, 32 (1993).
[8] H. Yu, G. Xiong, and J. Ma, J. TIT, 18–23, 17 (2001).
[9] W. Jiang, Z. Xu, and X. Zhang, Sm. Mater. Lett., 1042–1045, 61 (2007).
[10] A.S. Pradhan, J.I. Lee, and J.L. Kim, Med Phys, 85–99, 33 (2008).
[11] Y.X. Zhuang, Y. Lv, L. Wang, W.W. Chen, T.L. Zhou, T. Takeda, N. Hirosaki, and R.J. Xie, ACS Appl. Mater. Interfaces, 1854–1864, 10 (2018).
[12] H.B. Liu, B.L. Feng, L. Luo, C.L. Han, and P.A. Tanner, Opt. Mater. Express, 3375–3385, 6 (2016).
[13] Y.X. Zhuang, Y. Lv, Y. Li, T.L. Zhou, J. Xu, J. Ueda, S. Tanabe, and R.J. Xie, Inorg. Chem., 11890–11897, 55 (2016).
[14] A. Lecointre, A. Bessiere, A. Bos, and P. Dorenbos, J. Phys. Chem. C, 4217–4227, 115 (2011).
[15] L. Xiao, J. Zhou, G.Z. Liu, and L. Wang, J. Alloys Compd., 24–29, 712 (2017).
[16] S. Hufner and B. Judd, NY Acad. Press, 87–95, 32 (1979).
[17] J. Wu, N. Wang, V. Yan, and H. Wang, Nano Res., 1863–1877, 14 (2021).
[18] P. Dorenbos, J. Lumin., 155–176, 91 (2000).
[19] F. Clabau, A. Garcia, P. Bonville, D. Gonbeau, T. Le Mercier, P. Deniard, and S. Jobic. J. Solid State Chem., 1456–1461, 181 (2008).
[20] M. Ma, D. Zhu, C. Zhao, T. Han, S. Cao, and M. Tu, Opt. Commun., 665-668, 285 (2012).
[21] S.C. Gadam and S. Dhoble, J. Lumin., 23–26, 14 (2013).
[22] Y. Kojima, T. Aoi, and U. Tetsuo, J. Lumin., 42–45, 146 (2014).
[23] O.Y. Manashirov, E.M. Zvereva, V.B. Gutan, A.N. Gorgobiani, S.A. Ambrozevic, and A.N. Lobanov, Inorg. Mater., 487–491, 49 (2013).
[24] S. Shuang, D. Kai, K. Huang, and L. Cheng, Adv. Powder Technol., 1516–1519, 25 (2014).
[25] Z. Hua, L. Salamanca-Riba, M. Wuttig, and P.K. Soltani, J. Opt. Soc. Am. B, 1464–1469, 10 (1993).
[26] M.V. Nadezhkin, D.V. Orlova, S.A. Barannikova, and N.M. Mnikh, Rus. Phys. J., **65**, No. 3, 507 (2022).
[27] Z. Zhang, X. Xu, and J. Qiu, Spectrosc. Spectral Anal., 1486–1491, 34 (2014).
[28] X. Sun, J. Zhang, X. Zhang, Y. Luo, and Z. Hao, J. Appl. Phys., 013501, 105 (2009).
[29] F. Wang, Y.G. Tian, and Q. Zhang, J. Optoelectron. Laser, 1520–1525, 26 (2015).
[30] P. Li, Z. Yang, and Z. Wang, Chin. Sci. Bull., 973–977, 53 (2008).
[31] J. Sun, S. Li, L. Shi, Acta Phys. Sin.-CH ED, 243301–243309, 64 (2015).
[32] X. Liu, J. Zhang, X. Zhang, Z. Hao, J. Qiao, and X. Dong, Opt. Lett., 148–150, 38 (2013).
[33] M. Wang, X. Zhang, and Z. Hao, Opt. Mater., 1042–1045, 32 (2010).
[34] A.H. Krumpel and E.V. Kolk, J. Appl. Phys., 073505–073514, 104 (2008).